Analogue Electrical Circuit for Simulation of the Duffing-Holmes Equation

E. Tamaševičiūtė[1], **A. Tamaševičius**[2], **G. Mykolaitis**[2], **S. Bumelienė**[2], **E. Lindberg**[3]

[1]Department of Radiophysics, Faculty of Physics, Vilnius University
Saulėtekio ave. 9, LT-10222 Vilnius, Lithuania
elena.tamaseviciute@ff.vu.lt

[2]Plasma Phenomena and Chaos Laboratory, Semiconductor Physics Institute
A. Goštauto str. 11, LT-01108 Vilnius, Lithuania
tamasev@pfi.lt; gytis@pfi.lt; skaidra@pfi.lt

[3]Ørsted•DTU Department, 348 Technical University of Denmark
DK-2800, Lyngby, Denmark
el@oersted.dtu.dk

Abstract. We describe an extremely simple second order analogue electrical circuit for simulating the two-well Duffing-Holmes mathematical oscillator. Numerical results and analogue electrical simulations are illustrated with the snapshots of chaotic waveforms, with the phase portraits (the Lissajous figures) and with the stroboscopic maps (the Poincaré sections).

Keywords: nonlinear dynamics, chaos, electrical circuits.

1 Introduction

Electrical circuits generating complex and chaotic waveforms are convenient tools for imitating temporal evolution of nonlinear dynamical systems and for simulating differential equations. An example is the well known Mackey-Glass (MG) system [1, 2] given by a delay differential equation. An analogue electrical circuit, which imitates dynamical behaviour of the MG system, has been designed, built and investigated in [3,4]. It has been used to test experimentally various techniques developed to control chaos, specifically to stabilise either unstable steady states [4, 5] or unstable periodic orbits [6], to tune the correlation dimension of the strange attractor [7], to synchronize coupled infinite-dimensional hyperchaotic dynamical systems [8–10].

In this paper, we describe an extremely simple analogue electrical circuit dedicated for simulation the Duffing-Holmes (DH) equation [11–14]. There are three different approaches developed to process the DH equation and its solutions electrically. The first technique is a hybrid one making use of simulation the DH equation in a digital computer and a of digital-to-analogue conversion of the digital output for its further

analogue processing [15, 16]. The second method employs purely analogue means based on analogue computer design [17, 18]. For example, analogue computer has been used to simulate the DH equation and to investigate scrambling effects of chaotic signals in linear feedback shift registers [17, 18]. Later analogue computer, simulating the DH equation and displaying the electrical output voltages on the screen of an oscilloscope, has been suggested for chaos demonstration in the undergraduate student laboratories [19].

Evidently, the first and the second techniques are rather general and can be applied to other differential equations as well. In contrast, the third approach is based on building some specific analogue electrical circuit for a given differential equation. Despite its limitation to a specific equation, the "intrinsic" electrical circuits have an attractive advantage due to their simplicity and cheapness. Such circuits comprise only small number of discrete electrical components: resistors, capacitors, inductors, semiconductor diodes, also may include a single (sometimes several) operational amplifier.

We note, that any analogue computer is a standard collection of the following main blocks: inverting RC integrators, inverting adders, invertors, inverting and noninverting amplifiers, multipliers, and (if necessary) piecewise linear nonlinear units. Programming of the differential equations on an analogue computer is simply wiring these units according to strictly predetermined rules. Differences between the "intrinsic" analogue electrical circuits, simulating behaviour of dynamical systems, and the conventional analogue computers are discussed and emphasised in [20].

2 Equations and numerical results

The Duffing-Holmes oscillator is given either by the second order nonautonomous differential equation [11–14]:

$$\ddot{x} + b\dot{x} - x + x^3 = a \sin \omega t \tag{1}$$

or by an equivalent set of two first order nonautonomous equations

$$\dot{x} = y, \tag{2a}$$
$$\dot{y} = F(x) - by + a \sin \omega t \tag{2b}$$

with $F(x) = x - x^3$. In (1) and (2) b, a, and ω are the damping coefficient, the amplitude and the frequency of the external driving force, respectively. Equations (1) or (2) describe an externally driven particle in a two-well nonparabolic potential (sketched in Fig. 1):

$$W(x) = -\int F(x)dx = -\frac{x^2}{2} + \frac{x^4}{4}. \tag{3}$$

By adjusting any of the control parameters, namely a, ω or b, one can observe periodic and chaotic oscillations. Numerical results obtained from (2) using the software package MATHEMATICA are shown in Fig. 2 and Figs. 3–7.
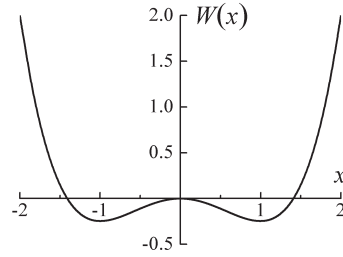
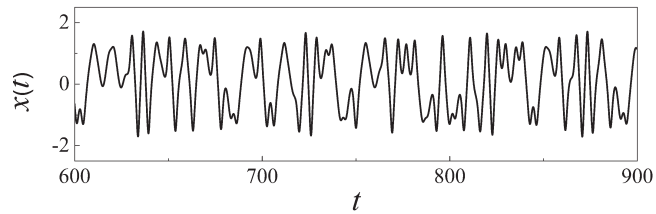Fig. 1. Two-well nonparabolic potential $W(x)$ from (3).

Fig. 2. Chaotic waveform $x(t)$ from (2). $a = 0.45, b = 0.1, \omega = 1.3$.
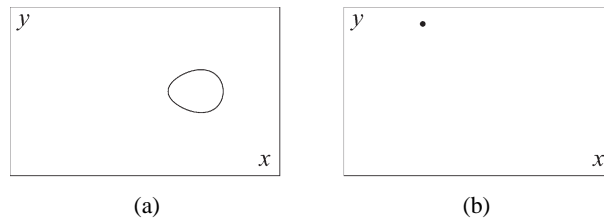
(a)   (b)

Fig. 3. (a) Phase portraits (Lissajous figures), (b) stroboscopic maps (Poincaré sections) from (2) at drive amplitude $a = 0.200$. $b = 0.1, \omega = 1.3$.
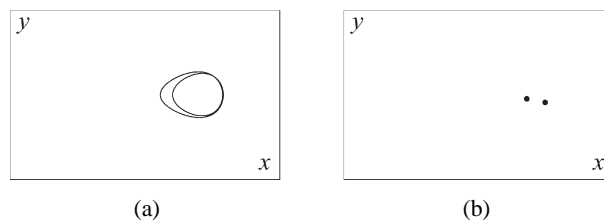
(a)   (b)

Fig. 4. (a) Phase portraits (Lissajous figures), (b) stroboscopic maps (Poincaré sections) from (2) at drive amplitude $a = 0.250$. $b = 0.1, \omega = 1.3$.
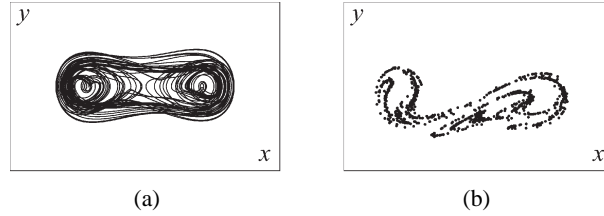
Fig. 5. (a) Phase portraits (Lissajous figures), (b) stroboscopic maps (Poincaré sections) from (2) at drive amplitude $a = 0.300$. $b = 0.1$, $\omega = 1.3$.
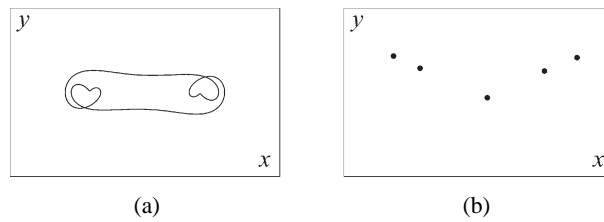

Fig. 6. (a) Phase portraits (Lissajous figures), (b) stroboscopic maps (Poincaré sections) from (2) at drive amplitude $a = 0.305$. $b = 0.1$, $\omega = 1.3$.
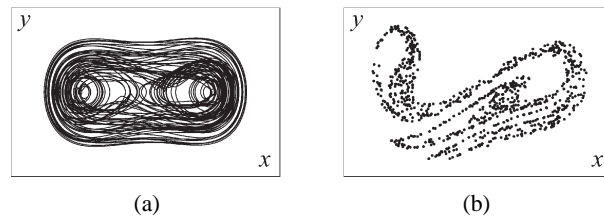

Fig. 7. (a) Phase portraits (Lissajous figures), (b) stroboscopic maps (Poincaré sections) from (2) at drive amplitude $a = 0.450$. $b = 0.1$, $\omega = 1.3$.

3 Electrical circuit and its equations

The suggested circuit is shown in Fig. 8. It is an externally driven damped RLC oscillator with all elements linear. The nonlinearity is involved by the positive feedback loop consisting of the resistor R3 and two diodes D1-D2. The operational amplifier OA plays the role of both, the buffer for the external sinusoidal force and the amplifying stage for the positive nonlinear feedback. The electrical circuit resembles the Young-Silva oscillator [21], but is essentially simpler. It includes a single operational amplifier, two diodes, and four resistors only, in contrast to the Young-Silva circuit containing four operational amplifiers, four diodes, and nine resistors.
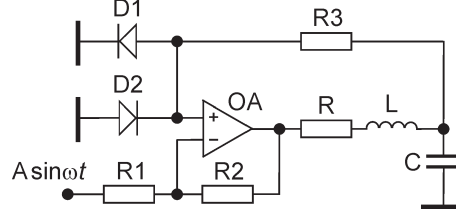
Fig. 8. Circuit diagram of the Duffing-Holmes oscillator.

Differential equations describing the circuit can be easily obtained using the Kirchhoff's laws:

$$C\frac{dV_C}{dt} = I_L, \tag{4a}$$

$$L\frac{dI_L}{dt} = F_E(V_C) - I_L R + A\sin(\omega t - \pi), \tag{4b}$$

where V_C is the voltage across the capacitor C and I_L is the current through the inductor L. In (4a) an assumption that $R_3 >> \rho = \sqrt{L/C}$ has been made. The constant phase π in the external force $A\sin(\omega t - \pi)$ can be omitted since it does not influence the dynamics of the system. The nonlinear function $F_E(V_C)$ can be given by a three-segment piecewise linear approximation:

$$F_E(V_C) = \begin{cases} -(V_C + kV^*), & V_C < -V^*, \\ (k-1)V_C, & -V^* \le V_C \le V^*, \\ -(V_C - kV^*), & V_C > V^*, \end{cases} \tag{5}$$

where $k = R_2/R_1 + 1$ is the gain of the amplifying stage and V^* is the voltage drop across an opened diode (for silicon diodes $V^* \approx 0.5\,V$ at 0.1 mA). It is convenient to choose $k = 2$ by setting $R_2 = R_1$. In (5) it is assumed that $R_{d0} >> R_3 >> R_{d1}$, where R_{d0} and R_{d1} are the resistances of the diode in the closed and the opened states, respectively. By introducing the following set of dimensionless variables and parameters

$$x = \frac{V_C}{2V^*}, \quad y = \frac{\rho I_L}{2V^*},$$

$$\frac{t}{\sqrt{LC}} \to t, \quad \omega\sqrt{LC} \to \omega,$$

$$a = \frac{A}{2V^*}, \quad b = \frac{R}{\rho}, \quad \rho = \sqrt{\frac{L}{C}},$$

equations convenient for analysis and numerical simulation are obtained:

$$\dot{x} = y, \tag{6a}$$

$$\dot{y} = F_E(x) - by + a\sin\omega t \tag{6b}$$

with

$$F_E(x) = \begin{cases} -(x+1), & x < -0.5, \\ x, & -0.5 \le x \le 0.5, \\ -(x-1), & x > 0.5. \end{cases} \tag{7}$$

The structure of the circuit equations (6) is exactly the same as of (2). The corresponding nonparabolic potential $W_E(x)$ has somewhat different form compared to (3) (especially at larger values of x) and is presented by a piecewise parabolic function (see also Fig. 9):

$$W_E(x) = -\int F_E(x)dx = \frac{1}{2} \begin{cases} (x+1)^2 - 0.5, & x < -0.5, \\ -x^2, & -0.5 \le x \le 0.5, \\ (x-1)^2 - 0.5, & x > 0.5. \end{cases} \tag{8}$$
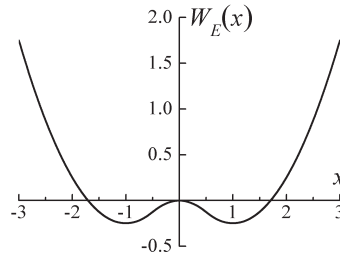

Fig. 9. Two-well nonparabolic potential $W_E(x)$ from (8).

4   SPICE simulation results

The circuit in Fig. 8 has been simulated using the "Electronics Workbench Professional" package which is based on the SPICE software. The following circuit element values have been used: $L = 19$ mH, $C = 470$ nF (resonance frequency $f_0 \approx 1.7$ kHz, $\rho \approx 200\,\Omega$), $R_1 = R_2 = R_3 = 10$ kΩ, $R = 20\,\Omega$, $f = \omega/2\pi = 1.5$ kHz. The operational amplifier OA is the LM741 type chip, the diodes D1 and D2 are general-purpose 1N4148 or similar type silicon devices. Simulation results are shown in Fig. 10 and Figs. 11–15.
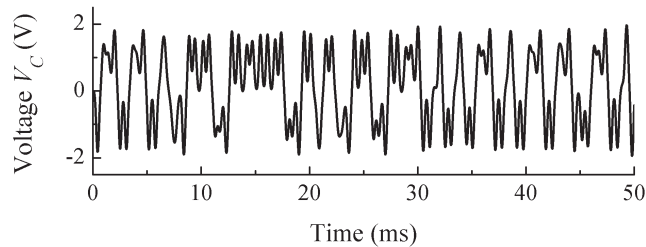

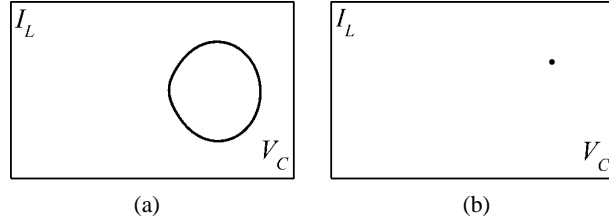Fig. 10. Chaotic waveform $V_C(t)$, $A = 240$ mV.

246

Fig. 11.   (a) Lissajous figures, (b) Poincaré sections at external drive amplitude $A = 120$ mV.
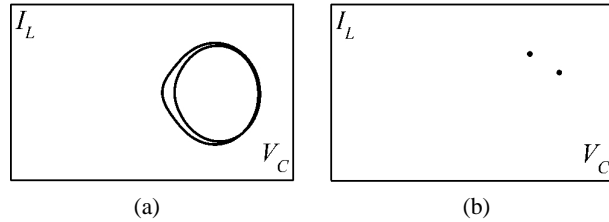

Fig. 12.   (a) Lissajous figures, (b) Poincaré sections at external drive amplitude $A = 140$ mV.
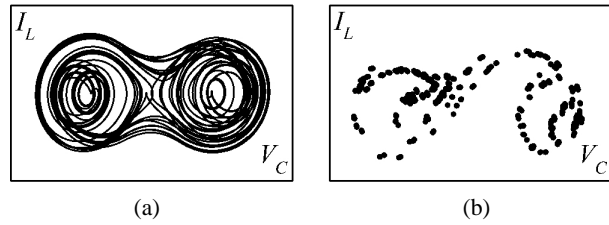

Fig. 13.   (a) Lissajous figures, (b) Poincaré sections at external drive amplitude $A = 160$ mV.
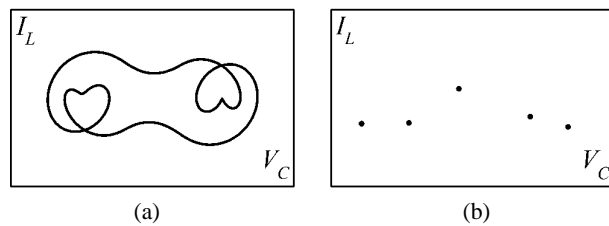

Fig. 14.   (a) Lissajous figures, (b) Poincaré sections at external drive amplitude $A = 196$ mV.
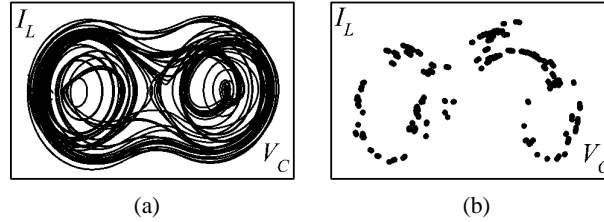
(a)   (b)

Fig. 15.   (a) Lissajous figures, (b) Poincaré sections at external drive amplitude
$A = 240$ mV.

5   Experimental results

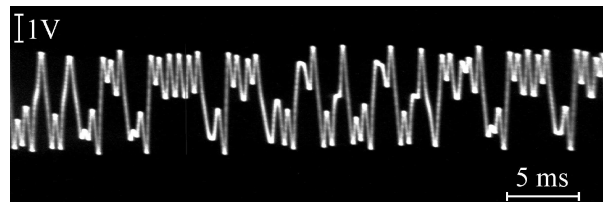A series of experimental results are presented in the Fig. 16 and Figs. 17–21.

Fig. 16. Experimental chaotic waveform $V_C(t)$. $A = 200$ mV.
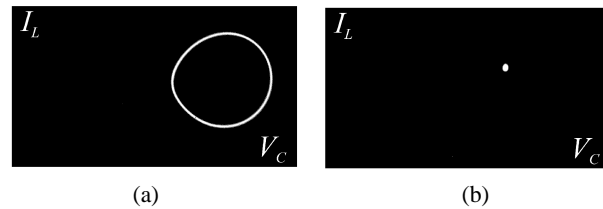

(a)   (b)

Fig. 17.   (a) Lissajous figures, (b) Poincaré sections at external drive amplitude
$A = 120$ mV.

Current $I_L(t)$ has been taken by means of a differential amplifier as a voltage drop $V_R(t)$ across resistor R. The plots represent either periodic or chaotic mode of oscillations. With the increase of the drive amplitude A the oscillator undergoes period-doubling route (Figs. 17, 18) to chaos, typical scenario for many nonlinear systems. Odd-period, e.g. the period-5 "two-heart" oscillations (Fig. 20) intersperse between the chaotic modes (Figs. 19, 21). The Poincaré sections have been taken at the sampling rate of one dot per period of the external driving force and contain 50 overlapping dots in the periodic and 1500 scattered dots in the chaotic plots.
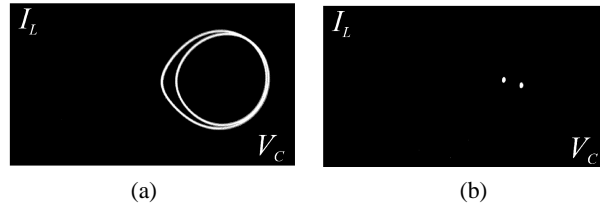
248

Fig. 18.   (a) Lissajous figures, (b) Poincaré sections at external drive amplitude $A = 140$ mV.
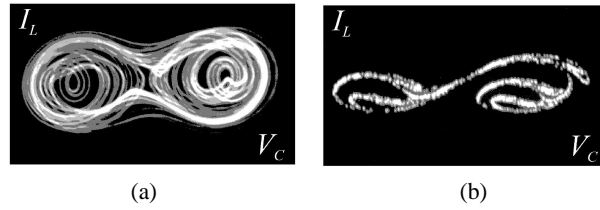

Fig. 19.   (a) Lissajous figures, (b) Poincaré sections at external drive amplitude $A = 150$ mV.
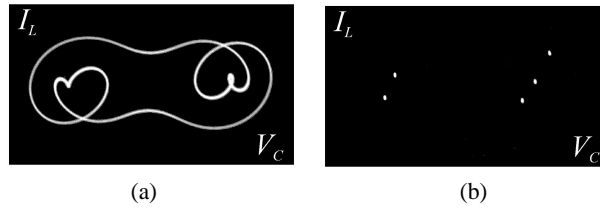

Fig. 20.   (a) Lissajous figures, (b) Poincaré sections at external drive amplitude $A = 160$ mV.
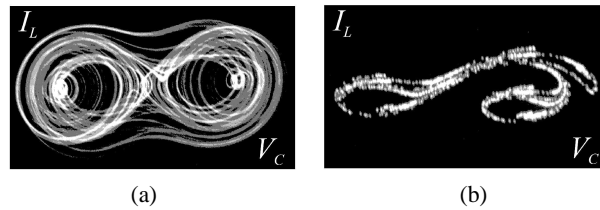

Fig. 21.   (a) Lissajous figures, (b) Poincaré sections at external drive amplitude $A = 200$ mV.

Agreement between numerical integration of (2), the SPICE simulation of the circuit in Fig.8 and experimental results taken from a hardware electrical circuit is quite good, including the "two-heart" attractor, which can be observed in a very small region of control parameters a, b and ω.

6 Concluding remarks

We have designed and investigated an electrical circuit, which can be treated as an electrical analogue of the Duffing-Holmes mathematical oscillator. The circuit is extremely simple, easy to build and operate. Nevertheless, it exhibits typical behaviour of chaotic systems, including period-doubling route to chaos, narrow odd-period windows in chaotic regime, etc. We have shown that many basic qualitative characteristics, such as the waveforms, the phase portraits (the Lissajous figures), and the stroboscopic maps (the Poincaré sections) can been easily taken in experiment. These characteristics coincide very well with the numerically obtained characteristics from the Duffing-Holmes equation. This allows us to conclude that dynamical behaviour of the Duffing-Holmes type systems is not sensitive to the details of the nonparabolic potential.

Very recently the developed analogue circuit has been employed in hardware experiments to test novel chaos control techniques [22, 23]. Stabilisation of unstable periodic orbits in the Duffing-Holmes chaotic oscillator, namely the orbits in the side wells of the two-well potential has been demonstrated experimentally in [22] by means of the resonant negative feedback method. Stabilisation of the central, torsion-free orbit (an orbit characterized by an odd number of positive Floquet exponents) by means of the unstable delayed feedback control technique has been verified experimentally in [23].

Acknowledgments

References

1. M. C. Mackey, L. Glass, Oscillation and chaos in physiological control system, *Science*, **197**, pp. 287–289, 1977.

2. J. D. Farmer, Chaotic attractor of an infinite-dimensional dynamical system, *Physica D*, **4**, pp. 366-393, 1982.

3. A. Namajūnas, K. Pyragas, A. Tamaševičius, An electronic analog of the Mackey-Glass system, *Phys. Lett. A*, **201**, pp. 42–46, 1995.

4. A. Namajūnas, K. Pyragas, A. Tamaševičius, Analog techniques for modeling and controlling the Mackey-Glass system, *Int. J. Bifurcat. Chaos*, **7**, pp. 957–962, 1997.

5. A. Namajūnas, K. Pyragas, A. Tamaševičius, Stabilization of an unstable steady state in a Mackey-Glass system, *Phys. Lett. A*, **204**, pp. 255–262, 1995.

6. A. Kittel, J. Parisi, K. Pyragas, Delayed feedback control of chaos by self-adapted delay time, *Phys. Lett. A*, **198**, pp. 433–436, 1995.

7. A. Namajūnas, A. Tamaševičius, Application of derivative feedback to control dimension of delay systems, *J. Techn. Phys.*, **37**, pp. 387–390, 1996.

8. A. Tamaševičius, A. Čenys, G. Mykolaitis, A. Namajūnas, E. Lindberg, Synchronisation of hyperchaotic oscillators, *Electron. Lett.*, **33**, pp. 2025–2026, 1997.

9. A. Tamaševičius, A. Čenys, G. Mykolaitis, A. Namajūnas, Synchronising hyperchaos in infinite-dimensional dynamical systems, *Chaos, Solitons and Fractals*, **9**, pp. 1403–1408, 1998.

10. A. Kittel, J. Parisi, K. Pyragas, Generalized synchronization of chaos in electronic circuit experiments, *Physica D*, **112**, pp. 459–468, 1998.

11. P. Holmes, A nonlinear oscillator with a strange attractor, *Phil. Trans. Roy. Soc. London A*, **292**, pp. 419–448, 1979.

12. F. C. Moon, *Chaotic Vibrations: An Introduction for Applied Scientists and Engineers*, Wiley, New York, 1987.

13. E. Ott, *Chaos in Dynamical Systems*, Cambridge University Press, Cambridge, 1993.

14. K. T. Alligood, T. D. Sauer, J. A. Yorke, *Chaos – an Introduction to Dynamical Systems*, Springer, New York, Berlin, 2000.

15. A. Namajūnas, A. Tamaševičius, Simple laboratory instrumentation for measuring pointwise dimensions from chaotic time series, *Rev. Sci. Instr.*, **65**, pp. 3032–3033, 1994.

16. A. Namajūnas, A. Tamaševičius, An optoelectronic technique for estimating fractal dimensions from dynamical Poincare maps, in: *Fractals in the natural and applied sciences, IFIP Trans. A: Computer Science and Technology*, **A-41**, pp. 289–293, 1994.

17. A. Namajūnas, A. Tamaševičius, G. Mykolaitis, A. čenys, Spectra transformation of chaotic signals, *Lith. J. Phys.*, **40**, pp. 134–139, 2000.

18. A. Namajūnas, A. Tamaševičius, G. Mykolaitis, A. Čenys, Smoothing chaotic spectrum of nonautonomous oscillator, *Nonlin. Phenom. Complex Syst.*, **3**, pp. 188–191, 2000.

19. B. K. Jones, G. Trefan, The Duffing oscillator: a precise electronic analog chaos demonstrator for the undergraduate laboratory, *Am. J. Phys.*, **69**, pp. 464–469, 2001.

20. T. Matsumoto, L. O. Chua, M. Komuro, The double scroll, *IEEE Trans. Circuits Syst.*, **32**, pp. 797–818, 1985.

21. Y.-Ch. Lai, A. Kandangath, S. Krishnamoorthy, J. A. Gaudet, P. S. de Moura, Inducing chaos by resonant perturbations: theory and experiment, *Phys. Rev. Lett.*, **94**, pp. 214101-1–4, 2005.

22. A. Tamaševičius, E. Tamaševičiūtė, G. Mykolaitis, S. Bumelienė, Stabilization of unstable periodic orbit in chaotic Duffing-Holmes oscillator by second order resonant negative feedback, *Lith. J. Phys.*, **47**, pp. 235–239, 2007.

23. A. Tamaševičius, G. Mykolaitis, V. Pyragas, K. Pyragas, Delayed feedback control of periodic orbits without torsion in nonautonomous chaotic systems: theory and experiment, *Phys. Rev. E*, **76**, pp. 026203-1–6, 2007.